

NEAR THRESHOLD FATIGUE CRACK GROWTH SIMULATION

T. Meshii¹, K. Ishihara² and K. Watanabe³

¹ Professor, Graduate School of Engineering, University of Fukui, Bunkyo, Fukui, Fukui, 910-8507, Japan

² Graduate Student, Graduate School of Engineering, University of Fukui, Bunkyo, Fukui, Fukui, 910-8507, Japan

³ Professor, Institute of Industrial Science, University of Tokyo, Komaba, Meguro-ku, Tokyo, 153-8505, Japan

ABSTRACT

In this paper, we performed the numerical simulations by the proposed simplified model to explain the decrease in threshold stress intensity factor (SIF) range ΔK_{th} due to high maximum SIF K_{max} . The results with tentative material resistances showed the validity of the proposed model, at least in the meaning that the decrease in ΔK_{th} by the increase with K_{max} was simulated.

1 INTRODUCTION

Since the pioneering work of Paris and Erdogan [1], the applied stress intensity factor (SIF) range ΔK has been known to be a major controlling parameter in fatigue crack growth (FCG) rate da/dN under small scale yielding conditions. At low FCG rates, da/dN - ΔK curve in log-log scale generally becomes steep and appears to approach a vertical asymptote that corresponds to the FCG threshold. ΔK corresponding to this asymptote is named as the threshold SIF range ΔK_{th} . Almost without exception, existing data show that the ΔK_{th} tends to decrease with increasing load ratio R [2]. Schmidt and Paris rationalized this behavior solely on the basis of the crack closure concept [3]. According to their model, we expect that the ΔK_{th} obtained by the K_{max} -constant test method (that ensures closure free conditions) is independent of K_{max} , and that it is constant. However, the decrease in ΔK_{th} due to high K_{max} is reported for some materials tested with K_{max} -constant methods [2]. To explain this decrease in ΔK_{th} due to high K_{max} , in this paper, we numerically modeled our qualitative model and ran numerical simulations to show the validity of our model.

2 SIMULATIONS

2.1 FCG algorism

From the observation of SEM fractographs and the assumptions we have made, we consider that the FCG mechanism is the same regardless of ΔK , based on the standpoint that microscopic cracks grow locally (such as in crystal grain) due to a cyclic or static mode fracture and the macroscopic crack front growth is observed as coalescences of microscopic cracks. In this case, the microscopic crack growth in any direction will contribute to macroscopic crack growth, because the crystal grain is separated [4]. Fig. 1 is a simplified model showing this mechanism, applied to FCG in an ASTM CT specimen.

In Fig. 1, each square (hereafter called as a cell) corresponds to a grain. We specify the location of a cell, for example, as i th row and j th column ($i = 1 \sim n_{\text{row}}, j = 1 \sim n_{\text{column}}$). In our model, we assume that the microscopic crack growth mechanism is selectively determined as cyclic or static mode failure, depending on the direction of the slip plane of the grain. Here we specify material resistances for cyclic and static mode failure as Δk_{Sij} and k_{Cij} , respectively. Another simplification is that the microscopic crack growth direction coincides with the macroscopic FCG direction. The depth of j th column is a_j and crack front is generally uneven as shown in Fig. 1. The nominal load in the simulation is controlled so that the maximum SIF is equal to the specified K_{max} and so that the SIF range ΔK - average crack length $a = (a_1 + a_{n_{\text{column}}})/2$ relationship for CT specimen

$$\Delta K = \Delta K_0 \exp(C(a - a_0)) \quad (1)$$

holds, same as that for standard ASTM FCG tests [5]. Here ΔK_0 is ΔK corresponding to the initial crack length a_0 and C is the ΔK -gradient, respectively.

Because of the uneven crack front with local length a_j , the local crack driving force in the j th column is distributed so that the maximum SIF and SIF range becomes $k_j, \Delta k_j$, respectively. Then these crack driving forces in the j th column are compared with the material resistances of the crack tip cells. Criteria we apply in our simulation is that there is a local crack growth in the case of $\Delta k_j > \Delta k_{Sij}$ or $k_j > k_{Cij}$, and on the other hand no local crack growth if $\Delta k_j < \Delta k_{Sij}$ and $k_j < k_{Cij}$. When $\Delta k_j < \Delta k_{Sij}$ and $k_j < k_{Cij}$ is satisfied for all columns, we finish the simulation and the nominal SIF range ΔK at this time is named as ΔK_{th} . The concrete algorithm of the FCG simulation is shown as a flow chart in Fig. 2. In the following, detailed procedures of the simulation are explained step by step, referring to Fig. 2.

2.1.1 Initial Setting

First, we specify CT specimen dimensions (B : thickness, W : width, a_0 : initial crack length, a_{END} : crack length for forced termination), quantities for specifying the size of a cell and its location (g : size of one cell in FCG direction, $n_{\text{row}}, n_{\text{column}}$), quantities relevant to material properties (E : Young's modulus, ν : Poisson's ratio, C_{Paris}, m : material constants of Paris law, $K_C, \Delta K_S$: basic material resistances for static and cyclic mode failure, respectively, α, β : the parameters to specify the scatter in material resistance of each cell, R : uniform random number seed).

Then the material resistances of each cell are randomly distributed by the following formula

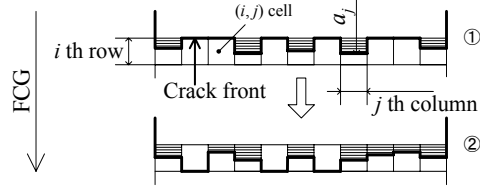


Figure 1: Our simplified mesoscopic crack coalescence FCG model [4]

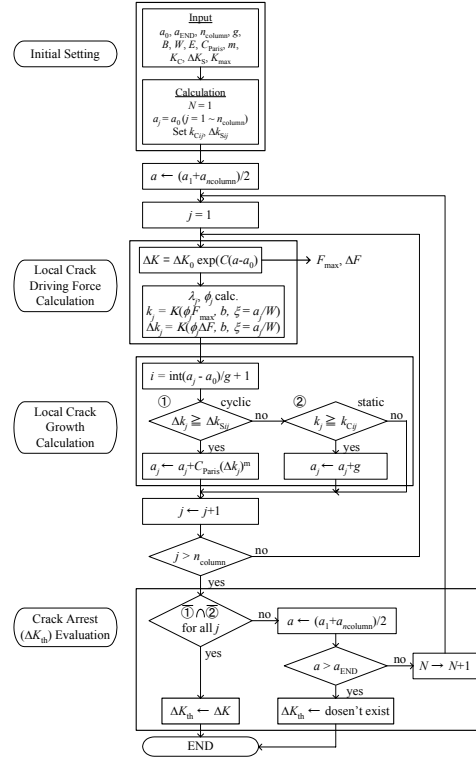


Figure 2: Flow chart of FCG algorithm

using the uniform random numbers ψ_{ij1} , ψ_{ij2} of $0 \sim 1$ generated with *RI*.

$$k_{Cij} = (\alpha + \beta \psi_{ij1})K_C \equiv \Psi_{ij1}K_C \quad (2)$$

$$\Delta k_{Sij} = (\alpha + \beta \psi_{ij2})\Delta K_S \equiv \Psi_{ij2}\Delta K_S \quad (3)$$

2.1.2 Local Crack Driving Force Calculation

As we described in section 2.1, the nominal load in the simulation is controlled so that the maximum SIF is equal to the specified K_{\max} and so that the SIF range ΔK - average crack length $a = (a_1 + a_{n_{\text{column}}})/2$ relationship for CT specimen satisfies eqn (1). The nominal maximum load F_{\max} and the load range ΔF corresponding to the nominal these crack driving forces can be counted backward from the SIF formula for the ASTM's standard CT specimen [5].

$$K(F, B, \xi = a/W) = \frac{F}{B \cdot W^{0.5} \cdot (1 - \xi)^{1.5}} \left[(2 + \xi) \cdot (0.886 + 4.64 \cdot \xi - 1332 \cdot \xi^2 + 1472 \cdot \xi^3 - 5.6 \cdot \xi^4) \right] \quad (4)$$

Then, in order to calculate the local crack driving force k_j and Δk_j in the crack tip of j th column, the load distribution coefficient ϕ_j is calculated by modeling the CT specimen with n_{column} slices of width $b = B/n_{\text{column}}$, crack length a_j and compliance λ_j as shown in Fig. 3. Since the slice model can be considered as a parallel spring,

$$\phi_j = 1 / \left(\lambda_j \sum_{l=1}^{n_{\text{column}}} (1 / \lambda_l) \right) \quad (5)$$

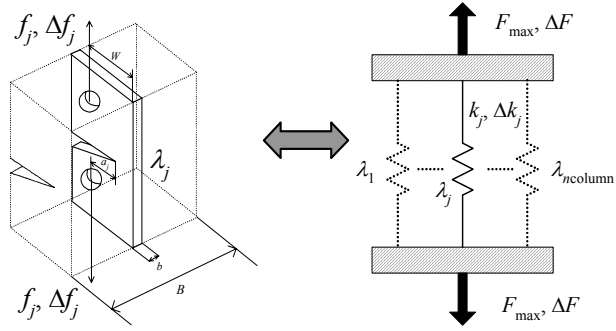


Figure 3: Slice model for stress redistribution

Here we used ASTM's following equation [5] for evaluation of λ_j ($\xi = a_j/W$),

$$\lambda_j = \frac{1 - \nu^2}{Eb} \left\{ \frac{19.75}{(1 - \xi)^2} (0.5 + 0.192\xi + 1.385\xi^2 - 2.919\xi^3 + 1.842\xi^4) \right\} \quad (6)$$

Since the maximum load and the load range of the local load of the slice of j th column is $\phi_j F_{\max}$ and $\phi_j \Delta F$, respectively, k_j and Δk_j can be calculated by the eqn (4) as follows.

$$k_j = K(\phi_j F_{\max}, b, \xi = a_j/W) \quad (7)$$

$$\Delta k_j = K(\phi_j \Delta F, b, \xi = a_j/W) \quad (8)$$

2.1.3 FCG Calculation

Once the local crack driving force of j th column is obtained, crack growth is evaluated for each column. First, row index i of the crack tip cell is evaluated using the material resistances for this cell. Then occurrence of local crack growth is judged by comparing the local crack driving force Δk_j , k_j with the material resistances of this cell Δk_{Sij} , k_{Cij} for all columns. Naturally, in this evaluation, we cannot evaluate the local crack growths by cyclic and static modes at the same time. If we simulate the load cycle faithfully, an idea to evaluate the crack growth by static mode and then that by cyclic mode might be considered better. However, it is reported that damage due to static mode failure does not necessarily occur in case slip occurs early in a load cycle [6]. Thus, we chose to first evaluate the occurrence of the cyclic mode failure and, in case of no cyclic mode failure, then evaluate the occurrence of static mode failure. We evaluated the amount of local crack growth in a certain cycle as follows:

- (1) In case of $\Delta k_j > \Delta k_{Sij}$, the amount of local crack growth in the j th column is evaluated as $C_{\text{Paris}}(\Delta k_j)^m$ according to the Paris law.
- (2) In case of $k_j > k_{Cij}$, the amount of local crack growth is assumed to be g , the size of a cell. (Note: There is a possibility that crack growth due to static failure mode is smaller than g , as a result that $k_j > k_{Cij}$ becomes not satisfied due to load redistribution. However, change in load distribution factor ϕ due to local crack growth calculated by eqn (4) was small, so we simply evaluated the amount of growth as g).

2.1.4 Crack Arrest Evaluation

Finally, crack arrest evaluation is performed after local crack growth evaluation is performed for all columns.

- (1) In case $\Delta k_j < \Delta k_{Sij}$ and $k_j < k_{Cij}$ are satisfied for all columns, we define that the crack has arrested. The nominal SIF range ΔK at this time is the ΔK_{th} that we wanted to obtain.
- (2) In case $a > a_{\text{END}}$ is satisfied as a result of FCG, we define that there was no ΔK_{th} .

If these conditions are not satisfied, local crack driving force calculation is again performed for the next cycle.

2.2 Preliminary calculation conditions and results

We carried out the simulation corresponding to our K_{max} -constant test for JIS carbon steel S55C by CT specimen whose size is $B = 12.5$, $W = 50$, and $a_0 = 18$ mm.

The size of a cell was set to $g = 0.03$ mm because the grain size was approximately that size. From this g and B , we set $n_{\text{column}} = 400$. Considering that the total amount of crack growth in a test was about 5 mm, we set $n_{\text{row}} = 168$. Crack length for simulation termination was set as $a_{\text{END}} = 21$ mm. As material constants, $E = 206$ GPa, $\nu = 0.3$, and $C_{\text{Paris}} = 1.35 \times 10^{-9}$, $m = 3.77$ obtained from tests [4] were used. The average value SIF for which the CT specimens experienced forced fracture was used as the basic material resistance K_C . On the other hand, ΔK_S was set as 3 MPam^{1/2} because test results of ΔK_{th} for low K_{max} was that value. Parameters to specify the scatter in material resistance of a cell was tentatively set as $\alpha = 0.5$ and $\beta = 1.0$ (namely, ψ_{ij1} and $\psi_{ij2} = 0.5 \sim 1.5$).

Constants in eqn (1) for load control was set as $\Delta K_0 = 12$ MPam^{1/2} and $C = -0.7$ mm⁻¹, that were used for our tests [4].

Here we tentatively specified the basic material resistances as aforementioned, though there are various possible combinations. Thus we first considered the influence of $K_C/\Delta K_S$ on da/dN and ΔK_{th} , under condition of identical scatter in material resistances (ψ_{ij1} and ψ_{ij2} for $RI = 81$). The results showed that $K_C/\Delta K_S$ had no effect on $da/dN - \Delta K$ curve nor ΔK_{th} , when K_{max}/K_C was set to a same value. Thus, the effect of K_{max} on $da/dN - \Delta K$ curve and ΔK_{th} was considered with constant $K_C/\Delta K_S$ hereafter.

The results are shown in Fig. 4 and 5. In Fig. 4, FCG rate da/dN was evaluated by the incremental polynomial method given in ASTM

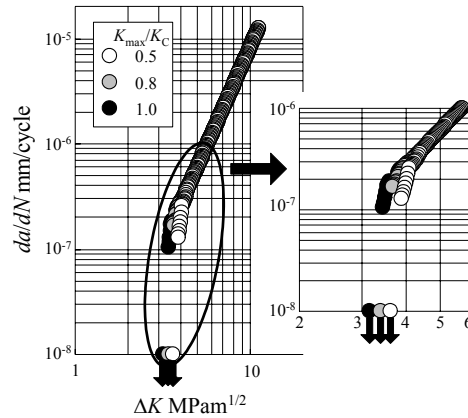


Figure 4: K_{max} -const. simulation results

E647 [5]. The ΔK corresponding to a plot for $da/dN = 10^{-8}$ mm/cycle is the nominal ΔK when the conditions of $\Delta k_j < \Delta k_{Sij}$ and $k_j < k_{Cij}$, were satisfied. This ΔK is called ΔK_{th} in this simulation.

We see from Fig. 4 that the da/dN - ΔK curves coincides for three K_{max}/K_C s in the range of $10^{-6} \sim 10^{-5}$ mm/cycle. On the other hand, we see the decrease in ΔK_{th} due to high K_{max} in the range below $da/dN = 10^{-6}$ mm/cycle. Thus we conclude that we can simulate the decrease in ΔK_{th} due to high K_{max} by our model [4], that was originally proposed to qualitatively explain the phenomenon observed for some materials under K_{max} -constant ΔK_{th} tests.

Fig. 5 is the fractured surfaces at the simulation end, corresponding to Fig. 4. The light gray, intermediate gray and black colored cell represent the no-fractured, cyclic-mode and static mode fractured cell, respectively. Digits with the scale on the right hand of the figure shows the crack length. We see in the cases of $K_{max}/K_C = 1.0$ that static mode fractured cells have appeared for $a > 19.5$ mm. On the other hand, in the case of $K_{max}/K_C = 0.5$, we see from Fig. 5 that the crack growth by the static mode failure has not occurred.

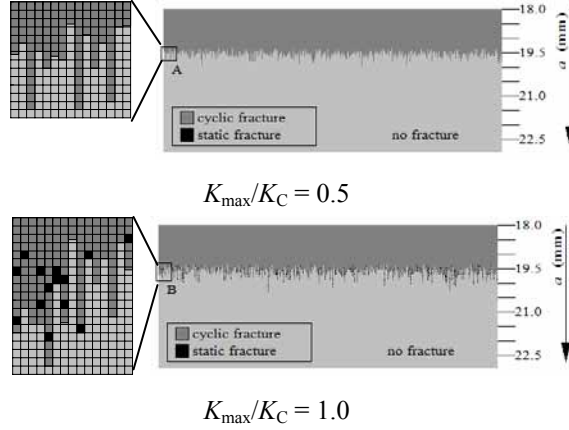


Figure 5: Fracture surface for Fig. 4

2.3 Detailed examination of the decrease in ΔK_{th} due to high K_{max}

Since phenomenon of the decrease in ΔK_{th} was observed when K_{max} was increased as $K_{max}/K_C = 0.5, 0.8$ and 1.0 in the aforementioned, we increased the numbers of simulations to examine this phenomenon in detail. We made simulations for six K_{max}/K_C in the range of $0.5 \sim 1.0$, graduated in 0.1 increments. For each K_{max}/K_C , 1352 material resistance distribution was considered by varying the uniform random number seed RI . For all cases, scatter in material resistance of a cell was tentatively set as $\alpha = 0.5$ and $\beta = 1.0$ ($\psi_{ij1}, \psi_{ij2} = 0.5 \sim 1.5$), identical with the aforementioned. The results are summarized as Fig. 6.

In Fig. 6, a closed circle with bars on upper and lower side represents the average $\mu \pm$ standard deviation σ of $\Delta K_{th}/\Delta K_S$ obtained from 1352 material resistance distributions. Maximum and the minimum values of $\Delta K_{th}/\Delta K_S$ are also shown in the figure for reference. We first see from the figure that the decrease in ΔK_{th} due to high K_{max} appears generally from the simulation and that the results in Fig. 4 were not special ones. Another finding is that the average value of $\Delta K_{th}/\Delta K_S$ seems to decrease linearly due to the increase in K_{max}/K_C . This linear relationship has been reported for carbon

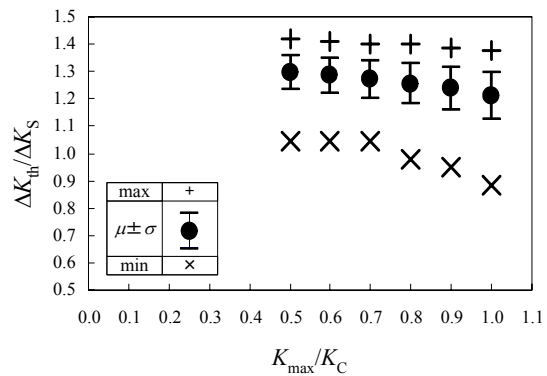


Figure 6: Relation of K_{max}/K_C and $\Delta K_{th}/\Delta K_S$ ($\alpha = 0.5, \beta = 1.0, \Psi_{ij1}, \Psi_{ij2} = 0.5 \sim 1.5$)

steel S55C [4] and for Ti and Al alloys [2].

In this meaning, though we used tentative values and made many assumptions, we conclude that our simplified FCG model [4] can simulate the decrease in ΔK_{th} due to high K_{max} .

3 DISCUSSION

As aforementioned in section 2.1, the local crack tip damage evaluation procedure was to first evaluate the occurrence of the cyclic mode failure, and in case of no cyclic mode failure, then evaluate the occurrence of static mode failure. As a result, the damage mechanism of a fractured cell is limited to the cyclic mode failure in the range of $\Delta K/\Delta K_S > 1.4$ (about 1.5, $a < 19.5$ mm), because a cell satisfying $\Delta k_j < \Delta k_{Sij}$ does not appear when scatter in the material resistance is set as $\psi_{ij1}, \psi_{ij2} = 0.5 \sim 1.5$. On the contrary, the evidence of a static mode failure has been found in the corresponding region of the actual specimen, although the number was few [4]. In the present simulation, we paid attention to FCG near the ΔK_{th} , and assumed that the static mode failure was an additional damage as a first trial. We admit that improvement is still necessary on selective damage algorithm.

In Fig. 6, we see that the average value of $\Delta K_{th}/\Delta K_S$ at a specific K_{max}/K_C was in the range of 1.2 ~ 1.3 when $K_{max}/K_C = 0.5 \sim 1.0$. Though not shown in the figure, $\Delta K_{th}/\Delta K_S$ was approximately 1.3 for $K_{max}/K_C < 0.5$. In addition, the minimum $\Delta K_{th}/\Delta K_S$ for $K_{max}/K_C \leq 0.5$ was larger than unity. One might have expected the single value of unity instead for this K_{max}/K_C . At this moment, we do not have a definite answer to explain the discrepancy between the simulation result and the expected value. However, we know from some additional simulations with smaller scatter in the material resistance that this average $\Delta K_{th}/\Delta K_S$ decreases from 1.3. We are still continuing investigation for this subject.

In our simulation, scatter in material resistances were tentatively set as $\Psi_{ij1}, \Psi_{ij2} = 0.5 \sim 1.5$. Our test results for the S55C show that ψ_{ij1} (variation of K_C) is 0.95 ~ 1.03 to average value, and ψ_{ij2} (variation in ΔK_{th} to a specific K_{max}) is 0.93 ~ 1.07 to average value [4]. In this meaning, the scatter in material resistances we used might be considered to be overestimating. However, to apply K_C or ΔK_{th} as material constants itself is an assumption. Thus, basic material resistances coupled with an appropriate scatter has to be discussed further to refine the model.

4 CONCLUSION

In this paper, we performed the numerical simulations by the proposed simplified model to explain the decrease in threshold stress intensity factor (SIF) range ΔK_{th} due to high maximum SIF K_{max} . The results with tentative material resistances showed the validity of the proposed model, at least in the meaning that the decrease in ΔK_{th} by the increase with K_{max} was simulated.

REFERENCES

- [1] Paris, P.C. and Erdogan, F., Trans. ASME, Ser. D, Vol. 85, pp. 528-534, 1963.
- [2] Boyce, B.L. and Ritchie, R.O., Engineering Fract. Mechanics, Vol. 68, pp. 129-147, 2001.
- [3] Schmidt, R.A. and Paris, P.C., ASTM STP 536, pp. 79-94, 1973.
- [4] Meshii, T., Ishihara, K. and Watanabe, K., Assessment for Decrease in Threshold Stress Intensity Factor (SIF) Range due to High Maximum SIF, Trans. JSME (A), in Japanese, Vol. 70, pp. 604-611, 2004.
- [5] ASTM, Standard test Method for Measurement of Fatigue Crack Growth Rate, Specification E647-93, American Society for Testing and Materials, Philadelphia, pp. 577-613, 1999.
- [6] Ritchie, R.O. and Knott, J.F., Acta Metallurgica, Vol. 21, pp. 639-648, 1973.